James Webb Space Telescope: Noise Results for the Multiplexers of the Mid-Infrared Instrument (MIRI)

Craig W. McMurtry, William J. Forrest, and Judith L. Pipher

University of Rochester, Rochester, NY, USA

ABSTRACT

The James Webb Space Telescope (JWST) will have several on-board instruments, of which the Mid-Infrared Instrument (MIRI) will cover imaging and low resolution spectroscopy in the 5-28 micron region. To achieve the many science goals for MIRI, the detector arrays must be capable of achieving high sensitivity. The primary obstacle to high sensitivity is the total noise. The total noise is often dominated by two main parts: the read noise of the multiplexer and the shot noise of the detector array's dark current. We present recent results of the measured read noise for several candidate multiplexers from the first Si-foundry run.

Keywords: Mid-IR, mid-infrared, detector array, Si:As, JWST, MIRI, low noise, low power, ROIC, Read Out Integrated Circuit, multiplexer

1. INTRODUCTION

We report on ROIC (Read-Out Integrated Circuit or multiplexer) testing under the JWST MIRI program.[1] The main requirements for the ROIC are low power ($< 1mW$) and low noise ($< 19e^-$ total noise in Fowler-8 sampled 1000 sec integration, which includes read noise from the ROIC and shot noise due to dark current from the Si:As detector array). Testing was conducted at the University of Rochester on bare ROIC SB-305s from the recent Lot 1 foundry run for the MIRI program. The details of the variations in the lot splits are Raytheon proprietary and will simply be referred to as lot split A and B. Four ROICs were optimized, calibrated and tested: part numbers SB-305-1-7-C2 and SB-305-1-3-C3 from lot split A, and part numbers SB-305-1-25-C2 and SB-305-1-25-C3 from lot split B.

For more information on the MIRI Si:As detector arrays, please see "1024×1024 Si:As IBC Detector Arrays for JWST MIRI", P. J. Love, et al. in these proceedings.

2. DATA

All data were taken with pixel enable time of $10.0\mu s$ and pixel-to-pixel time of $10.4\mu s$ (includes pixel de-select and next pixel select) for a total frame time of $2.80s$ for the full 1032×1024 ROIC, using 4 outputs. Our array controller electronics have a noise floor of $10\mu V$ for Fowler-1 sampling[2] (i.e. Correlated Double Sampling) and $\sim 3\mu V$ for Fowler-8 sampling.

2.1. SB-305-1-7-C2

The SB-305 has a common heritage (both in architecture and in foundry processing) with the SB-304, which performed well at 30K. Therefore initial functional and baseline tests were conducted on 1-7-C2 at 30K, where we have more familiarity with the operation and behavior of the ROICs. The performance of this ROIC at 30K was nearly identical to SB-290 and SB-304 ROICs that have been tested at the University of Rochester in the past.[3] The operating parameters (biases and clocks) are listed in Table 1. For the given $16\mu A$ of unit cell slew current and output load voltage, the signal output time constants are $\tau_{rise} = 1.3\mu s$ and $\tau_{fall} = 1.1\mu s$. We measured per pixel capacitance using visible light illumination and the noise squared versus signal method,[4] which assumes that the photons are absorbed at the integrating node and not at other locations in the unit cell. The inter-pixel capacitance was measured to be negligible.[5] The measured capacitance is 32.1fF at 30K, which is in good agreement with the expected ROIC capacitance based on comparison to total SCA capacitance for Si:As detector arrays[6] and InSb detector arrays,[3] which were hybridized to ROICs (SB-226, SB-291, SB-304) that were very similar to the SB-305. We measured the source follower gain curve using vRstOff and ϕRstOn both

Table 1. Voltages used and currents measured for biases and clocks for 1-7-C2. The currents have an uncertainty of $\pm 2\mu A$. Note: the actual Islew is $16\mu A$ total or $2\mu A/pixel$, see currents on Vdduc and Vssuc. For the voltages listed, a single value indicates the clock was operated at a constant level, while two values indicate the two rails used for the clock.

	T=30K		T=7.1K	
Bias or Clock	Voltage (V)	Current (μA)	Voltage (V)	Current (μA)
Vddcl	0.00	0	0.00	0
Vp	0.00	-17	0.00	-16
VnRow	-4.00	-1	-4.00	-1
VnCol	-3.20	+16	-3.20	+16
Vssuc	-0.50	-21	-0.50	-16
VidleRef	0.00	0	0.00	0
VslewRef	-4.22	+2	-2.60	+2
Vddout	-0.35	+102	-0.35	+95
Vssout	+2.50	-100	+2.50	-95
Vdduc	-3.20	+17	-3.20	+15
Vdet	-3.20	0	-3.20	0
VRowOff	-1.00	+2	-1.00	+4
VnStat	-6.00	0	-6.00	0
ϕC1	0.0 / -3.2		0.0 / -3.2	
ϕC2	0.0 / -3.2		0.0 / -3.2	
ϕR1	0.0 / -4.0		0.0 / -4.0	
ϕR2	0.0 / -4.0		0.0 / -4.0	
ϕRowOn	-1.0 / -4.0		-1.0 / -4.0	
ϕRstOn	-3.0 / -5.2		-3.0 / -5.2	
vRstOff	-3.0		-3.0	
ϕRefEn	0.0		0.0	
Vggcl	0.0		0.0	

set to "hard on" (−5.2V DC) while varying Vdduc versus Vout (see Figure 1). The read noise was measured using the "zero mean" method, i.e. the {standard deviation / $\sqrt{2}$ } in a sub-array from the difference of two dark images, where the expected mean is zero (see Figure 2).

We began low temperature (T=7K) operation using the same voltages as were used at 30K, with the exception of Vslewref, which was adjusted to provide the same slew current as previously used, namely $16\mu A$. The source follower gain curve can be seen in Figure 3. We were unable to use visible light illumination and the noise squared versus signal method to determine the capacitance at the lower temperature. A typical noise squared versus signal relationship is linear for small signals, however at 7.1K the relationship was far from linear. We have not investigated the cause for this experiment's failure, however excess noise or photon absorption in the ROIC at locations other than the integrating node could be factors. Therefore, we used the capacitance measured at 30K, C=32.1fF, to interpret the data obtained at 7.1K. We calculated a power dissipation of 0.11mW, derived from the sums of voltage × current. Using calorimetry to determine the power dissipation, we found that ROIC 1-7-C2 dissipates 0.50mW of power while in a 100% duty cycle mode which consisted of one full array row-by-row reset followed by two full array reads. While we have found good agreement in the past[7,3] between the two methods of determining the power dissipation, the disagreement here is likely due to excess currents on clock supply lines (particularly the reset) which were not included in the measurements of current. Typically clock currents are below our detection limit ($\sim 50\mu A$) for well-behaved ROICs operating at 30K, hence we did not measure the currents on the clock lines, but intend to do so in the near future. In our tests for read noise using the "zero mean" noise method, we obtained input referred read noise data versus Fowler sampling, see Figure 4,

For further information, E-mail: craig.mcmurtry@rochester.edu

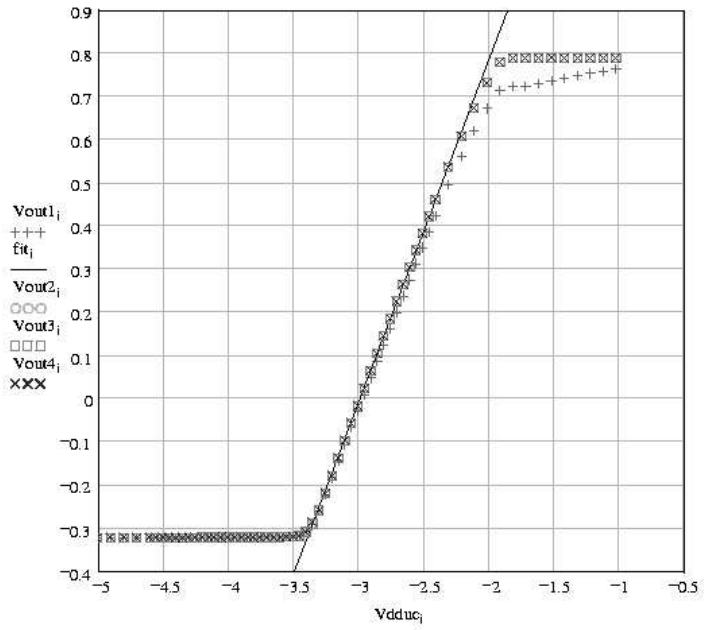

Figure 1. Source follower gain curve for output voltage versus Vdduc at 30K for ROIC 1-7-C2. The gain is 0.791 over the range of Vdduc = −3.3 to −2.1 V. Note: the first data set (plus symbol) included pixels in the 12 dead columns and hence departs from the other three data sets. The fourth data set is for the reference pixels only. The reference pixels and normal pixels are identical in terms of gain.

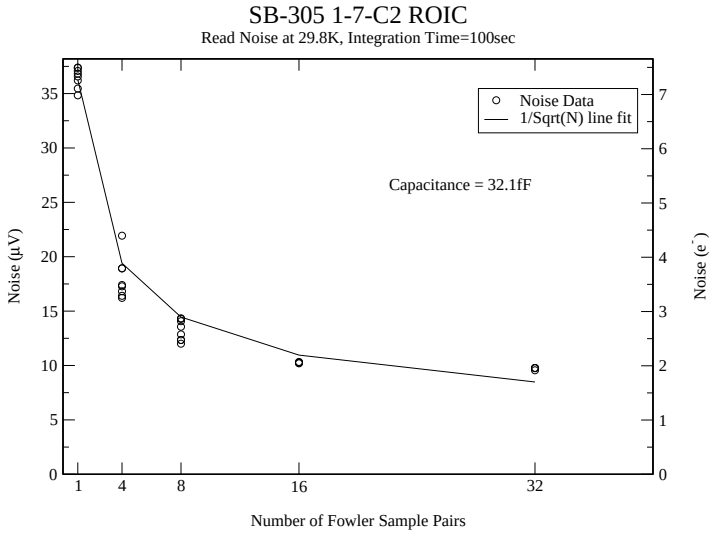

Figure 2. Read noise versus Fowler Sampling at 30K for ROIC 1-7-C2. Noise data were obtained using the zero mean method. The integration time was 100 seconds for all Fowler sampled images in these data. For the data at 30K, the capacitance was measured to be 32.1fF.

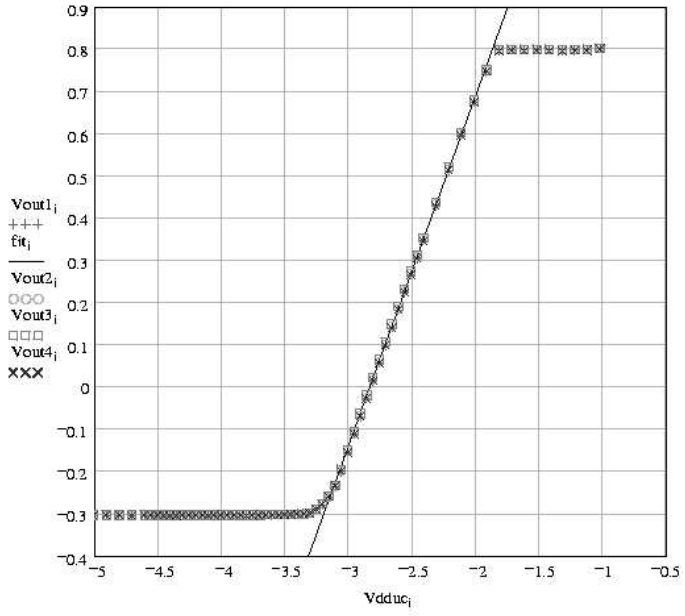

Figure 3. Source follower gain curve at 7K for ROIC 1-7-C2. The source follower gain is 0.828 at 7K, which is slightly higher than the gain at 30K. Also, note that the gain curve itself is shifted slightly toward more positive voltages at the lower temperatures (cf. Figure 1).

at $T = 7.1K$ and $T = 7.3K$: the data sets were statistically indistinguishable. During our testing, we noted that this ROIC *may* exhibit lower read noise at temperatures below 6.0K, however this was not investigated further since neither our present thermal connection nor the future cryostat on JWST is/will be capable of delivering sustained temperatures below 6.0K.

2.2. SB-305-1-3-C3

In order to be certain that the noise performance of part 1-7-C2 represents the expected noise performance of all ROICs from lot split A, we tested another bare ROIC from lot split A, namely 1-3-C3. The device 1-3-C3 performed nearly identically to 1-7-C2 in all respects at 7.1K, including read noise (see Figure 5).

2.3. SB-305-1-25-C2

We conducted tests at 30K, where we have experience with similar ROICs, to compare with data at lower temperatures. The operating parameters (biases and clocks) are listed in Table 2. Using $16\mu A$ of slew current (VslewRef) and $100\mu A$ of load current (Vddout) at 30K, the pixel output waveform's rise and fall time constant is $\tau = 0.9\mu s$. The source follower gain curve at 30K is shown in Figure 6. As with 1-7-C2, we measured the nodal capacitance and electronic conversion factor using the variance versus signal method at 30K. We obtained a pixel capacitance of $28.5fF$. This capacitance value, obtained at 30K, will be applied to all data on both 1-25-C2 and 1-25-C3 at 30K. We believe this is a good estimate for the capacitance of both devices since they are adjacent die from the same wafer. The read noise versus Fowler sampling using the "zero mean" method is shown in Figure 7.

The clock and bias voltages, which had worked well for 1-7-C2 at 7.1K, did not work for 1-25-C2, and instead caused self heating and large currents. We found that with the "on" rails of the row clocks and row biases (ϕR1,ϕR2, ϕRowOn and VnRow) set to -4.0V, there were large currents ($\sim 2.5mA$) flowing between VnRow and Vsub (analog ground). Changing the row clock and bias voltages toward more positive numbers, such as $-3.0V$, nearly eliminated the excess current and allowed the ROIC to be operated at 7.1K, i.e. smaller self heating.

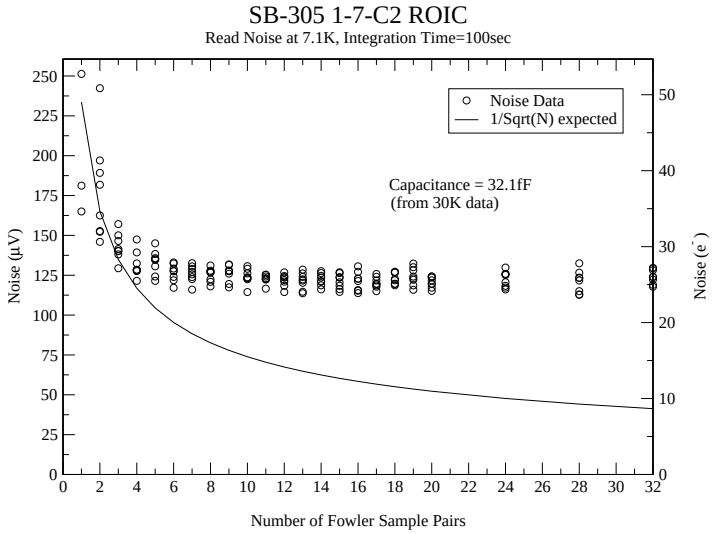

Figure 4. Input referred read noise versus Fowler Sampling at 7.1K for ROIC 1-7-C2. Noise data were obtained using the zero mean method. The integration time was 100 seconds for all Fowler sampled images in these data. For the data at 7.1K, we assumed a capacitance of 32.1fF (from 30K data) to convert from μV to e^-.

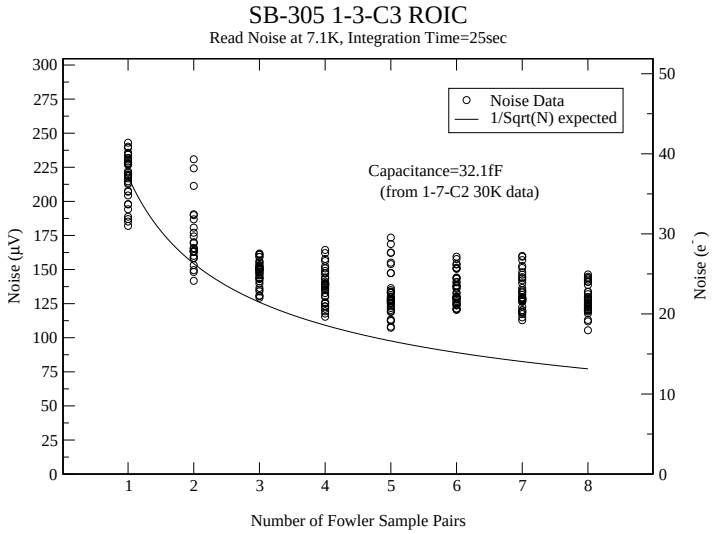

Figure 5. Input referred read noise versus Fowler Sampling at 7.1K for ROIC 1-3-C3. Noise data were obtained using the zero mean method. The integration time was 25 seconds for all Fowler sampled images in these data. For the data at 7.1K, we assumed a capacitance of 32.1fF (from 30K data) to convert from μV to e^-.

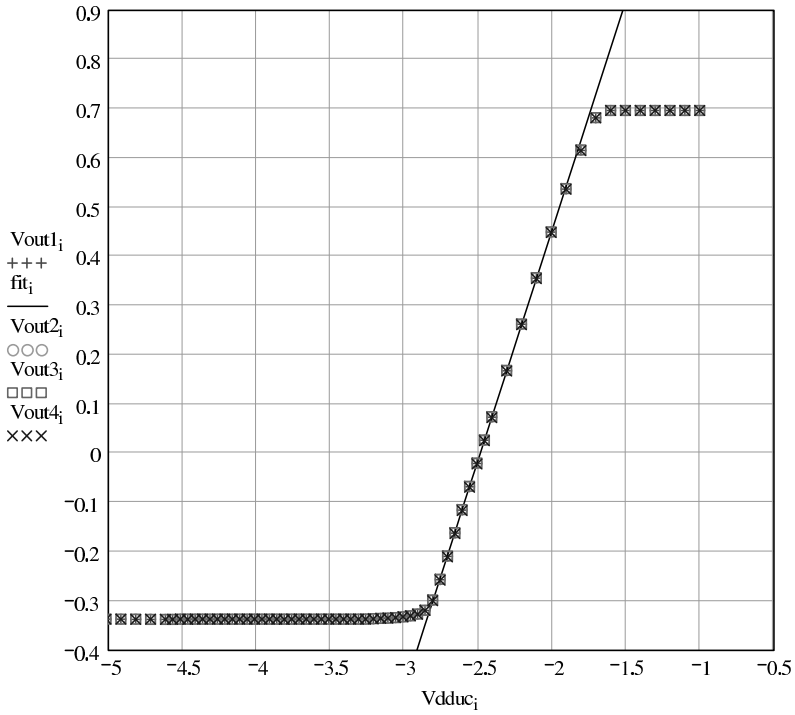

Figure 6. Source follower gain curve at 30.0K for ROIC 1-25-C2. The source follower gain is 0.934.

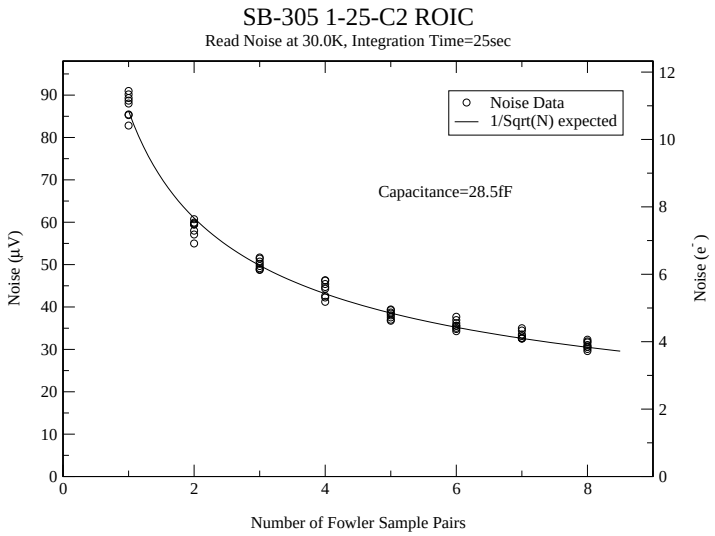

Figure 7. Input referred read noise versus Fowler Sampling at 30.0K for ROIC 1-25-C2. The integration time was 25 sec for all Fowler sampled images.

Table 2. Voltages used and currents measured for biases and clocks for 1-25-C2. The currents have an uncertainty of $\pm 2\mu A$. Note: the actual Islew is $16\mu A$ total or $2\mu A/pixel$, see currents on Vdduc and Vssuc. For the voltages listed, a single value indicates the clock or bias was operated at a constant level, while two values indicate the two rails used for the clock.

	T=30K		T=7.1K	
Bias	Voltage (V)	Current (μA)	Voltage (V)	Current (μA)
Vddcl	0.00	0	0.00	0
Vp	0.00	-17	0.00	-17
VnRow	-4.00	-3	-3.00	+20
VnCol	-3.20	+17	-3.20	+17
Vssuc	-0.50	-19	-0.50	-20
VidleRef	0.00	0	0.00	0
VslewRef	-3.84	+2	-2.60	+3
Vddout	-0.35	-104	-0.35	+96
Vssout	+2.50	+103	+2.50	-95
Vdduc	-2.60	+16	-2.60	+17
Vdet	-2.60	0	-2.60	0
VRowOff	-1.00	0	-1.00	+4
VnStat	-6.00	0	-6.00	0
ϕC1	0.0 / -3.2		0.0 / -3.2	
ϕC2	0.0 / -3.2		0.0 / -3.2	
ϕR1	0.0 / -4.0		0.0 / -3.0	
ϕR2	0.0 / -4.0		0.0 / -3.0	
ϕRowOn	-1.0 / -4.0		-1.0 / -3.0	
ϕRstOn	-3.0 / -5.2		-2.5 / -4.5	
vRstOff	-3.0		-2.5	
ϕRefEn	0.0		0.0	
Vggcl	0.0		0.0	

Further reduction in self heating was achieved by using more positive rails on both reset clocks. The operating parameters (biases and clocks) are listed in Table 2. For the given $16\mu A$ of slew current and output load voltage, the signal output time constants are $\tau_{rise} = 1.0\mu s$ and $\tau_{fall} = 0.9\mu s$. The source follower gain curve is shown in Figure 8. The capacitance measurement for 1-25-C2 also failed at 7.1K (see Section 2.1 for explanation). An assumed capacitance of 28.5fF was used based on 30K data for 1-25-C2, since the capacitance is not expected to change dramatically between the 30K and 7K temperatures. We measured the power dissipation to be 0.45mW of power using calorimetric methods. Noise data were taken using the "zero mean" method (see Figure 9) and also using the temporal method (see Figure 10). Additional read noise data were taken using the zero mean method for several 1000 sec Fowler-8 images, yielding $16.9e^-$ or $101.7\mu V$, which is somewhat higher than the 25 sec Fowler-8 results ($12.3e^-, 74.3\mu V$). The discrepancy in the read noise values for 25 sec versus 1000 sec is due primarily to 1/f noise contribution during the longer integrations. The read noise for 1000 sec integrations can be reduced by using better data processing routines that employ reference pixel corrections.[8]

2.4. SB-305-1-25-C3

For 1-25-C3, the voltages and currents used were nearly identical to those for 1-25-C2 (see Table 2), with the exception of $\phi RstOn = -2.5/-5.0V$. There is a minor short of approximately $70 - 100\mu A$ between $vRowOff$, $\phi RowOn$ and $vsub$. The source follower gain curve is shown in Figure 11. As previously noted (see Section 2.1 for explanation), the capacitance data were faulty, and thus we used an assumed capacitance of 28.5fF from 30K data for ROIC 1-25-C2. Given that ROIC 1-25-C3 is from the same wafer as 1-25-C2, it is plausible that the capacitances are identical for the two. The power dissipation is 0.60mW based upon calorimetric measurements.

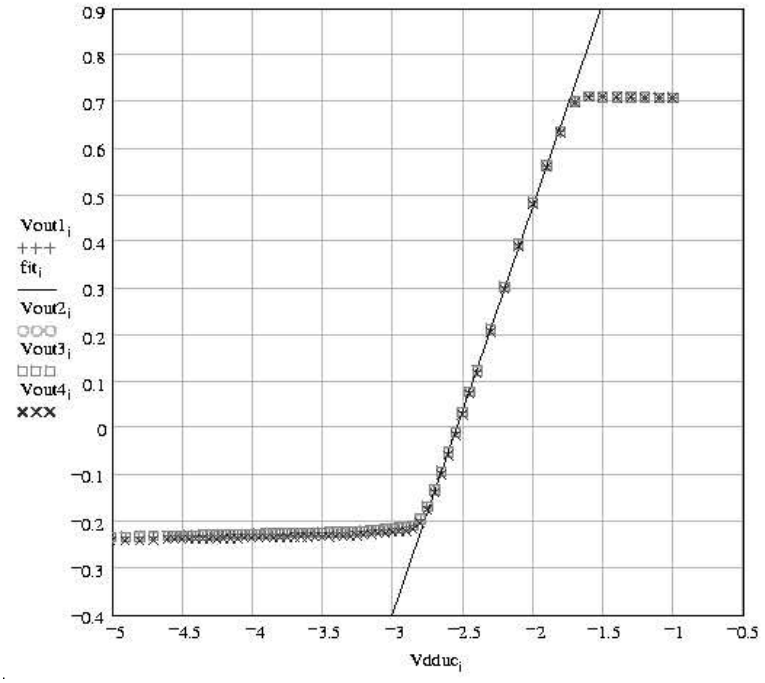

Figure 8. Source follower gain curve at 7.1K for ROIC 1-25-C2. The source follower gain is 0.871.

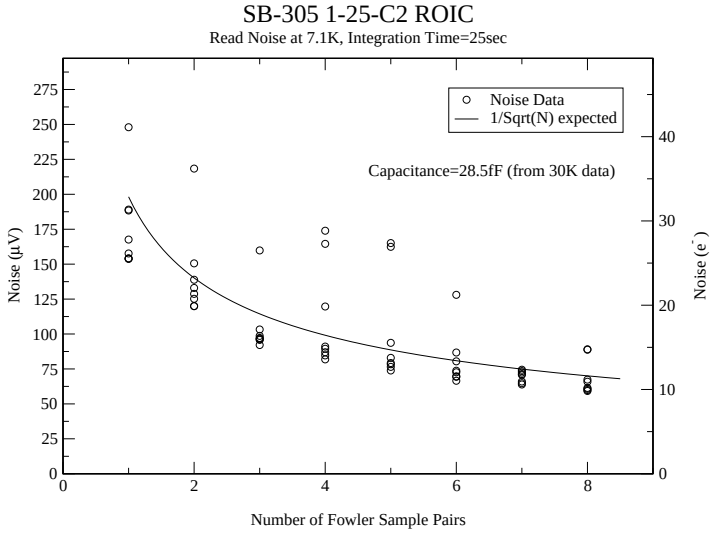

Figure 9. Input referred read noise versus Fowler Sampling at 7.1K for ROIC 1-25-C2. The integration time was 25 sec for all Fowler sampled images. Please note that one box was in a region that gave consistently higher noise due to excess row-banding noise in the first 80 rows. There is an occasional second point with higher noise due to cosmic ray hits (which were not filtered out). Therefore, we feel it is valid to ignore the 1-2 points outside the major groupings at each sampling.

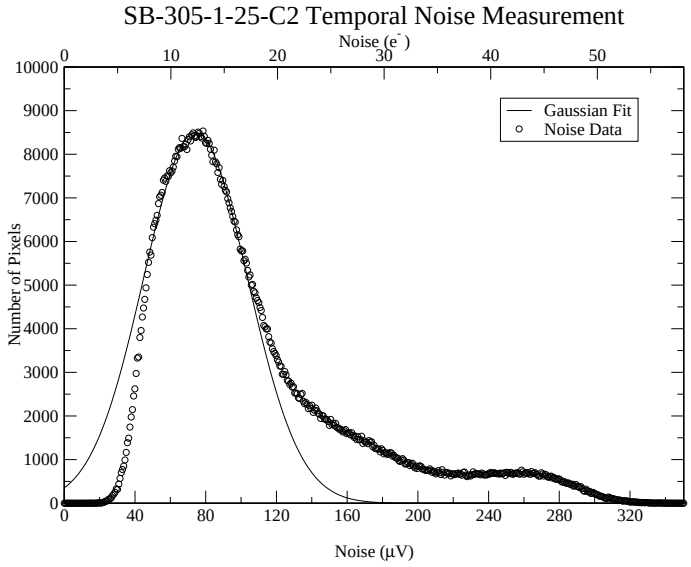

Figure 10. Input referred temporal noise per pixel at 7.1K for ROIC 1-25-C2. Shown is a histogram of per pixel noise sampled temporally using 50 images each with 25 sec Fowler-8 integrations. The mean of the Gaussian fit is $12.3e^-$ or $74.3\mu V$, input referred. The data were processed using an algorithm which used reference pixels to correct the DC offsets between images and used 4σ clipping to eliminate pixels affected by cosmic ray hits (typically for a given pixel, > 45 out 50 images did not have a cosmic ray hit). In addition, the reference pixels and 8 dead columns are not plotted here.

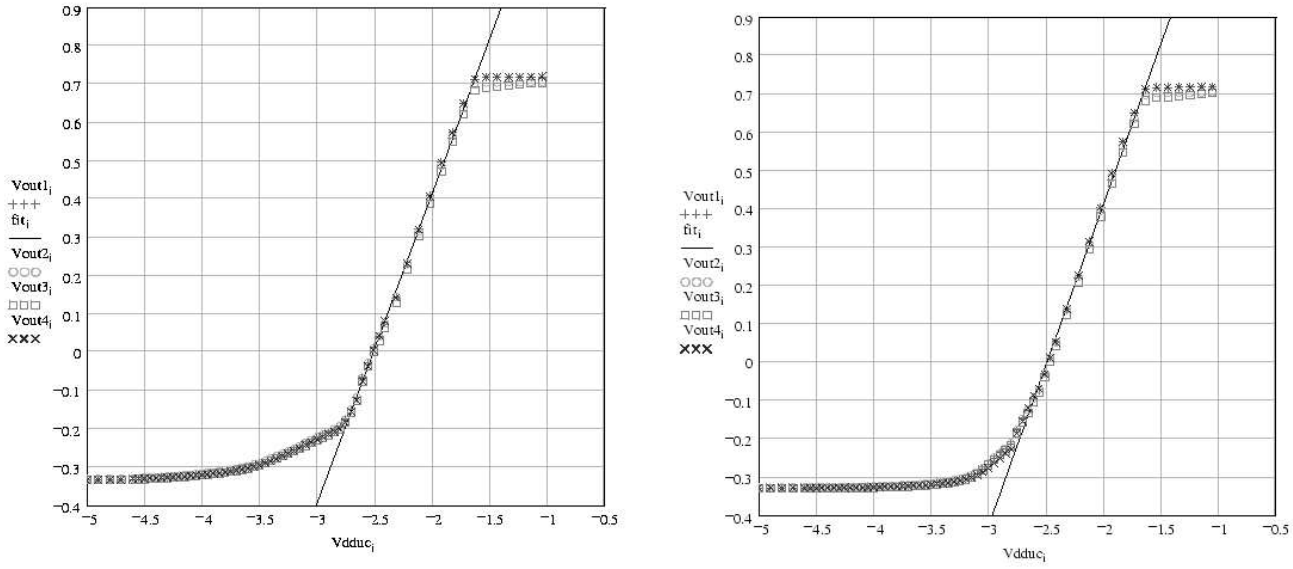

Figure 11. Source follower gain curve at 7.1K for ROIC 1-25-C3. The source follower gain is 0.838. **Left:** gain curve measured using both reset on rails set to $-4.5V$. Notice the non-linearity when $Vdduc = -3.0V$. **Right:** gain curve measured using both reset on rails set to $-5.0V$. Notice that the previous non-linearity has been reduced and the gain curve departs from the starvation level as expected.

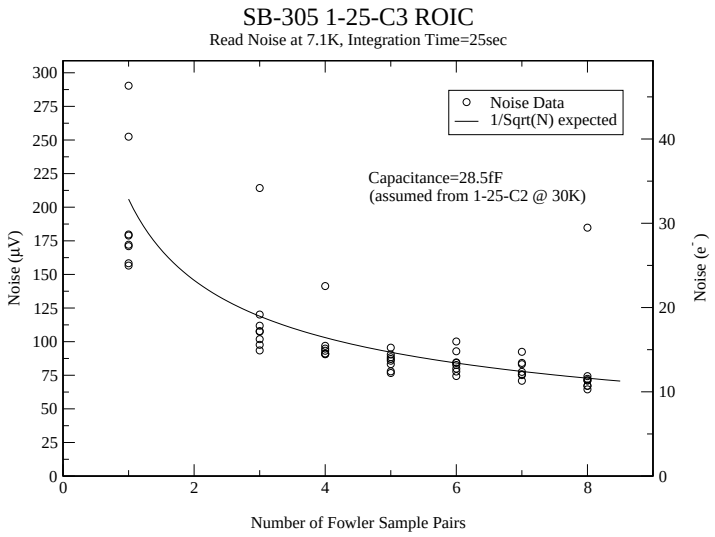

Figure 12. Input referred read noise versus Fowler Sampling at 7.1k for ROIC 1-25-C3. The integration time was 25 sec for all Fowler sampled images. Please note that one box was in a region that gave consistently higher noise due to excess row-banding noise in the first 80 rows. There is an occasional second point with higher noise due to cosmic ray hits (which were not filtered out). Therefore, we feel it is valid to ignore the 1-2 points outside the major groupings at each sampling.

Figures 12 and 13 show noise data taken using the "zero mean" method and the temporal method, respectively.

2.5. Comparison of Read Noises for ROIC Lot Splits

The read noise performance from the two ROIC lot splits is different even for the same temperature operation, as discussed above. The major factor, that determines the ROIC's noise performance, is the foundry processing (i.e. lot split variation), while some improvement in noise performance was obtained through clock and bias optimization for all the ROICs tested. In Figure 14, we show and discuss the noise power spectral density versus frequency data obtained for two ROICs. We applied a Fast Fourier Transform to a dark image to derive the noise power spectra. We did not use data obtained on a single pixel sampled at $10\mu s$ over an extended period of time (e.g. 100s). Instead, the dark images used were the same standard images used above in the read noise measurements. The application of an FFT to these dark images assumes that each pixel is identical to every other pixel, which is actually quite a good approximation as evidenced by the success of the "zero mean" method of noise measurement. Thus, a single image contains nearly identical pixels which are sampled every $10\mu s$ over the frame time.

It is necessary to note that the reference pixels were extremely important in correcting image-to-image drifts due to temperature and/or bias fluctuations. Without reference pixel corrections, the quoted noise for the temporal method in Section 2.3 would be $30-50\%$ higher. For all data processed, we used a simple subtraction method, i.e. the average value of all of the reference pixels was subtracted from the image. More complicated methods involve individual frame corrections in Sample-Up-The-Ramp mode and row-by-row fitted correction (see Rauscher *et al.*[8]). Such complex reference pixel correction methods may be of some use in reducing the noise for the long exposure (1000 sec Fowler-8 images), which have a higher than expected read noise compared with the 25 sec Fowler-8 images.

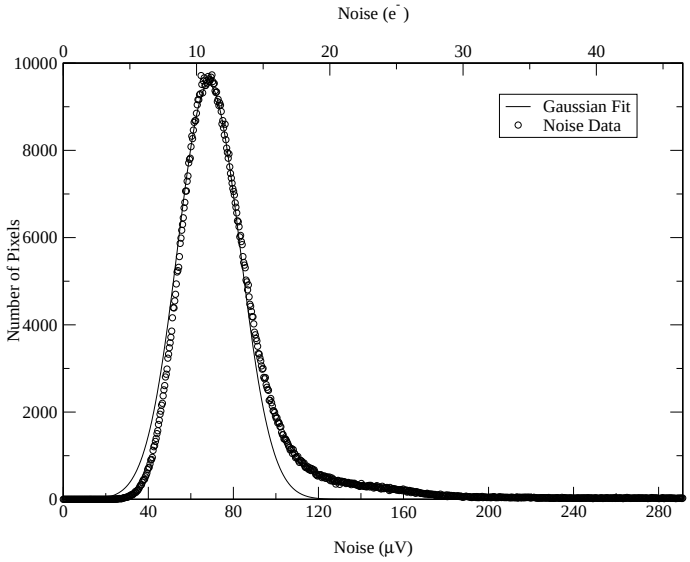

Figure 13. Input referred Temporal noise per pixel at 7.1K for ROIC 1-25-C3. Shown is a histogram of per pixel noise sampled temporally using 50 images each with 25 sec Fowler-8 integrations. The mean of the Gaussian fit is $11.0e^-$ or $68.5\mu V$, input referred. The data were processed using an algorithm which used reference pixels to correct the DC offsets between images and used 4σ clipping to eliminate pixels affected by cosmic ray hits (typically for a given pixel, > 45 out 50 images did not have a cosmic ray hit). In addition, the reference pixels, 6 dead columns and 2 dead rows are not plotted here.

Table 3. Table of number of pixels satisfying noise requirements for 1-25-C2 and 1-25-C3 from temporal noise data (see Figures 10 and 13). All data sets exclude reference pixels. Inoperable pixels, rows or columns are not excluded, i.e. those pixels are labeled as high noise and fail all requirements. The data set labeled as "1000^2" is for the central 1000^2 pixels, i.e. excluding a 12 pixel border. For the last column, the 1σ limits are derived from the FWHM of the Gaussian fits to the data in Figures 10 and 13. The 1σ limits are $4.9e^-$ for 1-25-C2 and $2.3e^-$ for 1-25-C3.

		Number of pixels with noise:			
ROIC	Data Set	$< 17e^-$	$< 18e^-$	$< 19e^-$	$< 19e^- + 1\sigma$
1-25-C2	1024^2	647143 (61.72%)	690463 (65.85%)	727305 (69.36%)	854852 (81.53%)
	1000^2	634242 (63.42%)	675867 (67.58%)	711191 (71.11%)	831996 (83.19%)
1-25-C3	1024^2	945634 (90.18%)	962071 (91.18%)	973785 (92.87%)	993586 (94.76%)
	1000^2	904387 (90.44%)	919140 (91.91%)	929654 (92.97%)	947714 (94.77%)

3. CONCLUSIONS

The read noise is nearly the same for both lot splits using Fowler-1 sampling. However, Lot Split A (1-7-C2 and 1-3-C3 ROICs) does not demonstrate the expected inverse root N behavior (where N is the number of Fowler sample pairs), whereas 1-25-C2 and -C3 ROICs from Lot Split B do exhibit the expected noise reduction behavior out to at least Fowler-8 which is promising. Both ROICs from wafer 25 performed within 10% of each other. There is good agreement between the major grouping at Fowler-8 in Figure 9 and the mean of the Gaussian fit in Figure 10. The read noise results for 1-25-C2 from both the "zero mean" method (see Figure 9) and the temporal method (see Figure 10) illustrate that there are some pixels which have higher noise than others. Results for the number of pixels satisfying the noise requirement of $< 19e^-$ are listed in Table 3. Those higher noise pixels are not distributed randomly, but instead tend to reside within the first 80 rows and the last 100

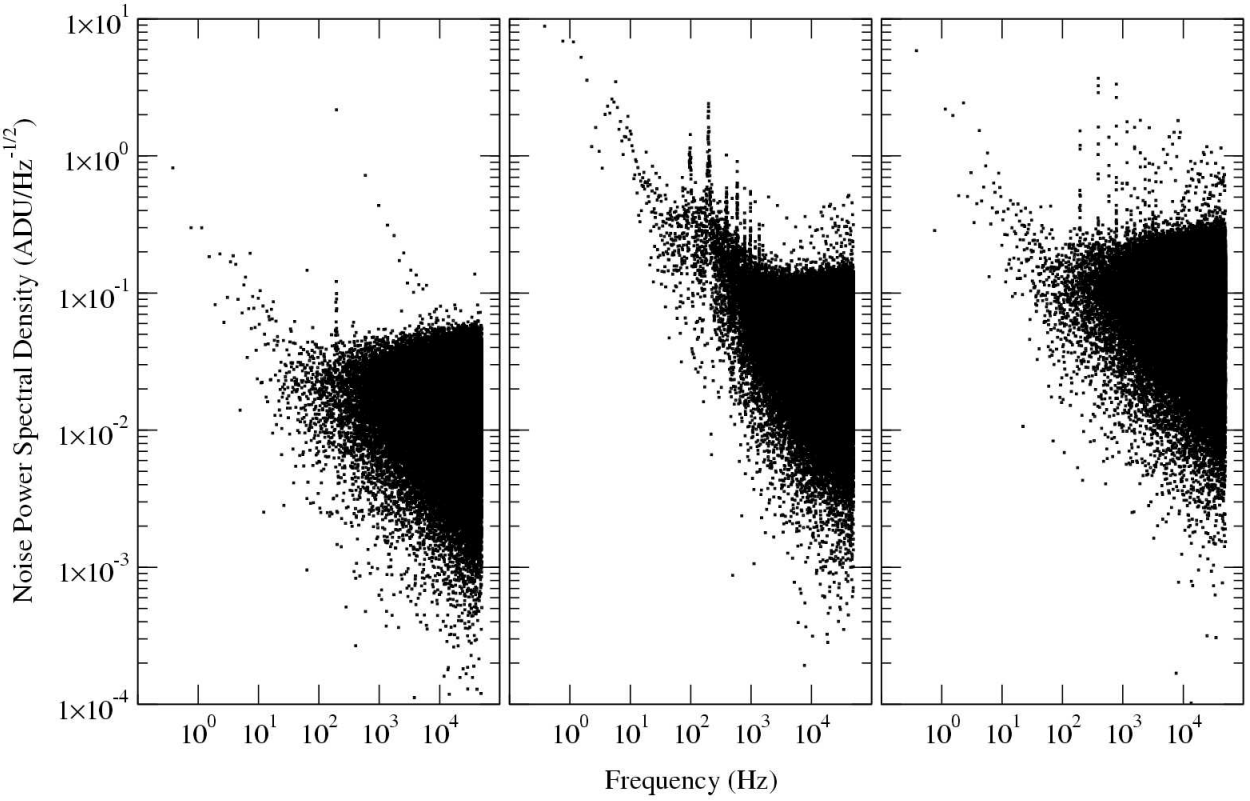

Figure 14. Noise Power Spectral Density versus Frequency. **Left:** Lot Split B ROIC at T=30K. **Center:** Lot Split B ROIC at T=7.1K. **Right:** Lot Split A ROIC at T=7.1K. At T=30K, both Lot Split A and B ROICs had very similar Noise Power Spectra. In general, the 1/f component provides a lower limit to the noise power spectral density at all frequencies, i.e. the noise is above and to the right of the 1/f slope. The white noise component is the filled (roughly) right triangle whose hypotenuse is coincident with the 1/f component and has a constant noise power over all frequencies, i.e. the upper portion of the triangle is horizontal for white noise. The remainder, that which is both above the 1/f component and above the upper horizontal part of the white noise component, is excess noise. In all three graphs, there is excess noise from the row shift register, i.e. an initial spike at approximately 195Hz with higher order multiples. In the left graph for the ROIC at T=30K, the noise overall is substantially lower than the noise at T=7.1K as well as having less total noise power due to row clock noise. When comparing the two ROICs' noise power spectra at T=7.1K (center and right), one can see that both have significant row clock noise at low frequencies. However, only the lot split A ROICs (right) have a large noise power due to row clock noise at higher frequencies and have a large non-white noise component at higher frequencies. For lot split A ROICs, this large noise power at higher frequencies is non-white and causes the departure from $1/\sqrt{N}$ noise reduction for increasing numbers of samples (see Figure 4).

Table 4. This table shows a comparison of the noise for different number of Fowler samples taken at different temperatures.

		Average Read Noise (e^-) at T=30K		Average Read Noise (e^-) at T=7K	
	Lot Split	Fowler-1	Fowler-8	Fowler-1	Fowler-8
1-7-C2	A	7	2.5	45	27
1-3-C3	A			38	22
1-25-C2	B	11	4	30	12.3
1-25-C3	B			35	11.0

columns. This grouping points toward the need for further optimization of the clocks and biases. We believe that further optimization will lead to a tighter, more nearly Gaussian distribution and possibly slightly lower average noise. In fact, Figure 13 shows a tighter Gaussian distribution, owing to a better optimized reset voltage. Further optimization will involve adjustment to the timing of reset and row clocks.

The average noise for each ROIC at the two temperatures tested are shown in Table 4. In our testing of bare ROIC lot splits for both the SB-226 and SB-291 development (unpublished data: Raytheon proprietary), we found similar trends in terms of noise performance at a given temperature. For example, at 30K the lot split A ROICs had lower noise (factor of 1.5 - 2.5) than the lot split B ROICs, while the opposite was true at 7K.

In conclusion, the measured read noise for a 1000sec, Fowler-8 sampled dark image from a lot split B SB-305 ROIC is $16.9e^-$ and does meet the JWST MIRI total noise requirement of less than $19e^-$ (based upon an assumed dark current $< 0.08e^-/sec$).

REFERENCES

1. C. McCreight, M. Greenhouse, D. Figer, R. Martineau, M. Jurotich, and B. Seery, "NGST ISIM Technology Development Requirements and Goals for NGST Detectors," *http://www.ngst.nasa.gov/doclist/bytitle.html* **Document 641**, 2001.
2. A. M. Fowler and I. Gatley, "Noise reduction strategy for hybrid IR focal-plane arrays," in *Proc. SPIE, Infrared Sensors: Detectors, Electronics, and Signal Processing*, T. S. Jayadev, ed., **1541**, pp. 127–133, 1991.
3. C. W. McMurtry, W. J. Forrest, A. C. Moore, and J. L. Pipher, "James Webb Space Telescope: Characterization of Flight Candidate NIR InSb Detector Arrays," in *Proc. SPIE, Focal Plane Arrays for Space Telescopes*, T. J. Grycewicz and C. R. McCreight, eds., **5167**, pp. 144–158, 2003.
4. L. Mortara and A. Fowler, "Evaluations of CCD: Performance for Astronomical Use," *Proc. SPIE, Solid State Imagers for Astronomy* **290**, pp. 28–30, 1981.
5. A. C. Moore, Z. Ninkov, and W. J. Forrest, "Interpixel Capacitance in Nondestructive Read-out Focal Plane Arrays," in *Proc. SPIE, Focal Plane Arrays for Space Telescopes*, T. J. Grycewicz and C. R. McCreight, eds., **5167**, pp. 204–215, 2003.
6. K. Ennico, M. McKelvey, C. McCreight, R. McMurray, R. Johnson, A. Hoffman, P. Love, and N. Lum, "Large Format Si:As IBC Array Performance for NGST and Future IR Space Telescope Applications," in *Proc. SPIE, IR Space Telescopes and Instruments*, J. C. Mather, ed., **4850**, pp. 890–901, 2002.
7. J. Wu, W. J. Forrest, J. L. Pipher, N. Lum, and A. Hoffman, "Development of infrared focal plane arrays for space," *Review of Scientific Instruments* **68**, pp. 3566–3578, 1997.
8. B. J. Rauscher, D. F. Figer, M. W. Regan, L. E. Bergeron, J. Balleza, R. Barkhouser, G. Greene, S. Kim, S. McCandliss, E. Morse, R. Pelton, T. Reeves, U. Sharma, P. Stemniski, H. S. Stockman, and M. Telewicz, "Ultra-Low Background Operation of Near-Infrared Detectors Using Reference Pixels for NGST," in *Proc. SPIE, IR Space Telescopes and Instruments*, J. C. Mather, ed., **4850**, pp. 962–970, 2002.